Computed Tomography Studies of Lung Ventilation and Perfusion

Eric A. Hoffman and Deokiee Chon

Departments of Radiology and Biomedical Engineering, University of Iowa, Iowa City, Iowa

With the emergence of multidetector-row computed tomography (CT) it is now possible to image both structure and function via use of a single imaging modality. Breath-hold spiral CT provides detail of the airway and vascular trees along with texture reflective of the state of the lung parenchyma. Use of stable xenon gas wash-in and/or wash-out methods using an axial mode of the CT scanner whereby images are acquired through gating to the respiratory cycle provide detailed images of regional ventilation with isotropic voxel dimensions now on the order of 0.4 mm. Axial scanning during a breath hold and gating to the electrocardiogram during the passage of a sharp bolus injection of iodinated contrast agent provide detailed images of regional pulmonary perfusion. These dynamic CT methods for the study of regional lung function are discussed in the context of other methods that have been used to study heterogeneity of lung function.

Keywords: computed tomography, functional, quantitative, xenon; pulmonary blood flow; pulmonary perfusion; pulmonary ventilation

The primary role of the lung is to deliver oxygen from the air into the venous blood and to extract carbon dioxide from the blood at the same air–blood interface. Thus, matching of ventilation and perfusion within various regions of the lung is critical for adequate gas exchange. To understand the etiology of physiologic manifestations of lung pathology, it has been critical to understand the interrelationship between regional lung ventilation and regional lung perfusion and to interrelate these two functional parameters to lung structure. Imaging methods are emerging to provide powerful new tools in the quest for this understanding.

To infer nonuniform lung ventilation, a large amount of early work was based on simple nitrogen wash-out curve (1) imaging of the distribution of inhaled radioactive xenon gas (2), regional strain measured via implanted lung markers used in conjunction with biplane X-ray fluoroscopy (3–6), as well as regional density changes seen with X-ray computed tomography (CT) imaging of the lung and multiple static inflation steps (7, 8). For the measurement of pulmonary perfusion, radioactive gases (9–11), radiolabeled microaggregated albumin, and radioactive microsphere injection (12, 13) have been extensively used. Ventilation–perfusion relationships in lung compartments, without specific knowledge of where the compartments are or whether they are contiguous, have been studied via the multiple inert gas elimination technique (14). These early studies provided significant insights into lung function and served to establish the notion that ventilation and perfusion are heterogeneous but well matched under normal conditions. A revolution in X-ray CT methods, taking advantage of multidetector-row CT (MDCT), has now provided a means of quantitatively studying regional lung ventilation and perfusion in conjunction with acquisition of highly detailed information regarding lung structure. Simultaneously there has been a demand for objective, quantitative tools with which to assess regional lung structure and function as new methods for intervening in lung disease emerge. Surgical and nonsurgical interventions in late-stage emphysema have increased the demand for methods by which to identify subsets of patients likely to benefit from the interventions, transbronchial biopsies have increasingly required imaging-based methods of guidance, and therapies targeted at interventions early in the pathologic development of a disease require tools more sensitive than the pulmonary function test or the radiologist's subjective visual reading of a radiograph or CT scan to identify subjects needing early intervention and to evaluate the effectiveness of the intervention. As interest increases in delivering drugs via inhalation rather than injection, it becomes critically importance to be able to evaluate the effect of these drugs, such as insulin, on the lungs. Elsewhere in this issue, the reader will find discussions of magnetic resonance imaging, positron emission tomography (PET), and bronchoscopy, and discussions of methods for assessing anatomic details of the lung, such as airway geometry. In this article, we focus on methods for imaging ventilation ($\dot{V}$), perfusion ($\dot{Q}$), and $\dot{V}/\dot{Q}$ via CT methodologies, and we place these methods into context with other methods that have provided our current understanding of lung structure–function relationships.

MDCT

Early studies of the lung via CT imaging used a one-of-a-kind scanner developed at the Mayo Clinic (Rochester, MN), known as the dynamic spatial reconstructor (15–17). This scanner provided the means of capturing a volumetric image of the lung in as short a time as 1/60th of a second, with increased resolution provided by widening the scan aperture, and typically apertures of 4/60th of a second were used for assessing regional perfusion, which was calculated by the injection of iodinated contrast agent and scanning gated to the cardiac cycle as the contrast agent passed through the lung with the lung held at a fixed volume (18). Regional ventilation was estimated by assessing regional density changes in the lung as the lung was inflated and imaged at each static inflation step (7, 8). Because early CT scanners required up to 2 to 5 s to acquire projection data for the reconstruction of a single slice of the lung, little work was done to assess lung function in the clinical arena via this modality, and the modality gained a reputation of being strictly targeted at imaging anatomic features. Imatron Corporation (South San Francisco, CA) developed a scanner known initially as the Ultrafast or Cine CT, later referred to as the electron beam CT (EBCT) (19), which provided scan apertures of 50 ms and up to eight slices of 7-mm thickness each or thin, single 3-mm-thick sections gathered in 100 ms. The table step took 1 to 2 s and thus images of the full lung could be acquired during a static breath hold on the order of 40 s. The EBCT scanner had a spatial resolution of approximately 10 line pairs per centimeter.

(*Received in original form September 12, 2005; accepted in final form September 21, 2005*)

Supported by National Institutes of Health grants HL-064368 and HL-060158.

Correspondence and requests for reprints should be addressed to Eric A. Hoffman, Ph.D., Department of Radiology, University of Iowa Carver College of Medicine, 200 Hawkins Drive, Iowa City, IA 52240. E-mail: eric-hoffman@uiowa.edu

The color figures for this article are on p. 506.

Proc Am Thorac Soc Vol 2. pp 492–498, 2005
DOI: 10.1513/pats.200509-099DS
Internet address: www.atsjournals.org

Although this modality provided a useful research tool with which to assess both ventilation (20) and perfusion (21), this application of the EBCT remained impractical for use in the clinical arena. At the end of the 1990s a new class of CT scanners emerged, known as MDCT scanners. These scanners had reduced rotation times of 0.5 s and initially acquired four simultaneous thin (1- to 1.5-mm) sections. Using a spiral mode of scanning, highly detailed anatomic images of the lung could be acquired volumetrically with a breath hold of 40 s, but with an increased spatial resolution on the order of 24 line pairs per centimeter. Because scan aperture (rotation time) was down to 0.5 s it was now possible to image axially and gate the scanner to the cardiac cycle during a breath hold such that blood flow measures could be assessed similarly to those acquired earlier via the dynamic spatial reconstructor (18, 22) or later by the EBCT scanner (23–25). These MDCT scanners have rapidly evolved to such as point that they can now acquire 64 slices in a single rotation and a rotation is completed in as little as 0.3 s. Volumetric images are now acquired with a breath hold of 5 s or less and axial blood flow assessment is widened such that up to 4 cm of z-axis coverage is achievable. It is clear that z-axis coverage will soon widen as rotation times will continue to drop. A fully equipped MDCT scanner suite is shown in Figure 1 and includes a xenon delivery device (Enhancer 3000; Diversified Diagnostic Products, Houston, TX), a high-powered contrast injector (MEDRAD, Indianola, PA), and a physiologic monitoring system (IntelliVue; Philips Medical Systems, Bothell, WA). The xenon Enhancer 3000 allows for the rebreathing of xenon gas, the scrubbing of CO_2, and maintenance of the O_2 and Xe concentration constant. The contrast injector provides 950 to 1,200 psi of pressure to deliver 0.5 cm^3 of iodinated contrast agent per kilogram in 2 to 3 s, with injection into the superior vena cava. The *inset* to Figure 1 shows a micro-CT scanner (microCAT II; Siemens Medical Systems, Knoxville, TN), which allows for imaging mice at 18-μm resolution, such that one can visualize alveoli *in vivo*. This is briefly discussed at the conclusion of this article.

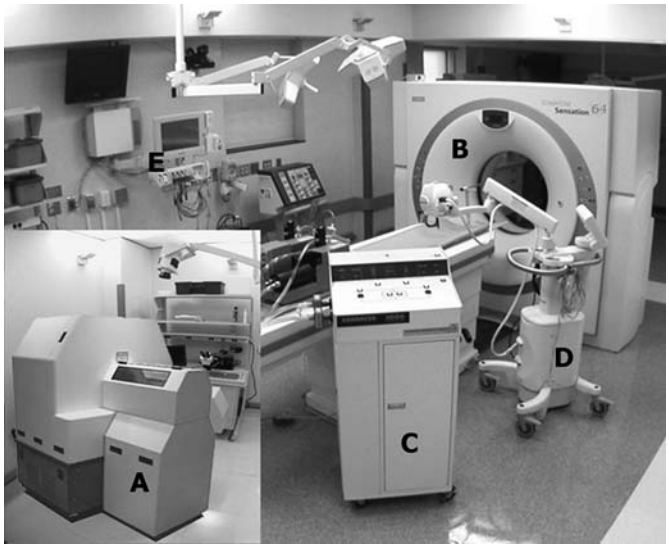

Figure 1. Composite image of computed tomography (CT) scanners and associated equipment used in functional imaging of the lung. (*A*) Micro-CT scanner (microCAT II; CTI Molecular Imaging, Knoxville, TN); (*B*) multidetector-row CT scanner (SOMATOM Sensation 64; Siemens Medical Solutions, Forscheim, Germany); (*C*) xenon delivery device (Enhancer 3000; Diversified Diagnostic Products, Houston, TX); (*D*) high-powered contrast injector (Mark V; MEDRAD, Indianola, PA); (*E*) physiologic monitoring system (IntelliVue patient monitor; Philips Medical Systems, Bothell, WA).

IMAGING TECHNIQUES TO STUDY PULMONARY VENTILATION AND PERFUSION

Perfusion Measurement Methods

Although multiple methods are currently available to measure pulmonary perfusion quantitatively, they have relative limitations and are not used routinely in clinical applications.

The technique using radiolabeled red blood cells or serum albumin macroaggregates was applied to evaluate regional pulmonary transit time and blood flow by determining the amount of radiation emitted from a specific region of interest (ROI) (26). Also, regional perfusion can be measured by using insoluble radioactive gas with a low blood–gas partition coefficient, such as ^{133}Xe, on the basis of the concept that radioactivity distributes within alveolar in proportion to local perfusion (27).

Regional pulmonary perfusion has been measured on the basis of the concept that the number of microspheres trapped in an ROI is proportion to regional perfusion (28). After microspheres are injected intravenously, fluorescence intensities are measured by extracting fluorescent dye and dye concentration is determined by fluorimetry. This method has relatively poor spatial resolution (because of the need to acquire enough spheres for a meaningful estimate of flow and because of the difficulty of dicing the lung too finely).

Mijailovich and coworkers (29) provided the theoretical background for positron emission tomographic (PET) measurement of pulmonary perfusion from $^{13}N_2$ concentration during apnea. When nitrogen gas arrives in the pulmonary capillaries, most of the tracer gas diffuses into the alveolar air space during a first pass because of its low solubility in blood and tissue; regional tracer content during apnea is proportional to regional $\dot{Q}$. Brudin and coworkers (30) calculated pulmonary perfusion by measuring ventilation obtained during continuous inhalation of ^{19}Ne and $\dot{V}/\dot{Q}$ during constant intravenous infusion of ^{13}N in saline solution. This technique has reduced temporal and spatial resolution, compared with magnetic resonance imaging (MRI) and CT. More recently, Venegas and colleagues (31–33) used PET to measure perfusion. Furthermore, with the modeling they employ, they have made perfusion estimates that have allowed them to predict blood gases. Others (34) have used PET to measure perfusion with ^{15}O-labeled water and also to measure perfusion via PET with macroaggregates of labeled albumin (effectively microspheres that degrade in the body and can be used in humans). With the implementation of commercial PET CT scanners, it is now possible to begin to use these modalities to cross-validate each other and to begin to design studies that best make use of the unique capabilities offered by each modality. Furthermore, with the more limited availability of PET scanners, it may be of interest to identify how CT may provide the same information as PET. CT clearly has resolution such that it is able to evaluate flow in, for instance, nodules of sizes not visible in a PET image.

Wolfkiel and Rich (25) measured myocardial blood flow by EBCT, using a single-compartment model of indicator transport. The basic concept of their model is that flow is proportional to maximum enhancement. Wu and coworkers, using the dynamic spatial reconstructor, applied this model in pigs to measure pulmonary blood flow and showed a good correlation with microsphere-based flow measurements. The assumption of the model used is that tissue accumulation of indicator must be nearly complete before the onset of indicator wash-out. Wolfkiel and Rich tested this assumption by comparing time–density curves of the pulmonary outflow tract, lung parenchyma, and

aortic outflow tract. According to their article, even if the arrival time on the left side of the circulation was slightly before the peak lung parenchymal enhancement time, estimation of the amount of wash-out was minimal (2.7 ± 5.3%) at the time of peak lung contrast enhancement, suggesting that the assumption of no indicator wash-out is valid for pulmonary blood flow measurements made with central intravenous bolus injections. This model using CT has been applied by other investigators studying both animals and humans (35). Won and coworkers (36) demonstrated the ability to use dynamic CT imaging to extract the signal within a single voxel related to microvascular blood flow, thus demonstrating the ability to estimate perfusion parameters at or near the very interface that provides gas exchange in the lungs. This was done by assessing the time–attenuation curve in the feeding pulmonary artery and in the peripheral parenchymal regions to then extract the transfer function, which expresses the mathematical function serving to convert the arterial curve into the parenchymal curve. It was observed that the transfer function was bimodal; and it was concluded that if the first mode reflected the partial-volume small arteries in a voxel, and the second mode reflected the partial-volume microvascular bed, then one could eliminate the first portion of the transfer function, reconvolve the arterial curve with just the second portion of the transfer function, and thus derive a time–attenuation curve reflecting microvascular perfusion. An example of perfusion measures obtained in a human nonsmoker and in a human smoker is shown in Figure 2 (p. 506) with scanning having been achieved via MDCT (SOMATOM Sensation 16; Siemens Medical Solutions, Forscheim, Germany). Note the increased heterogeneity of perfusion in the smoker, possibly representing disruption of normal perfusion via inflammatory processes.

Use of pulmonary perfusion measures is largely limited to date to the assessment of pulmonary emboli (37–41) or the characterization of lung nodules (42). No study to date has used quantitative measures (ml/min/g) for clinical assessment of the lung. Studies assessing pulmonary emboli and lung nodules have relied on slow, prolonged infusions of contrast simply to evaluate enhancement of the local blood pool. This has erroneously been termed "perfusion." It is in fact "perfused blood volume."

MRI has been used to evaluate pulmonary perfusion in animals and humans (43). Perfusion can be evaluated by analyzing enhancement after intravenous injection of contrast material (typically gadolinium). CT has significant potential for measuring highly regionalized pulmonary blood flow on the basis of first-pass indicator dilution principles, using iodinated contrast medium (44). The measurement of blood flow in brain (45) and myocardium (24), using CT, was introduced in the early 1980s. However, the measurement of blood flow has been limited by the long scan time, long interscan delays, and a lack of nondiffusible indicators (46, 47). The indicator must satisfy several criteria in order to allow the application of first-pass indicator dilution theory: (*1*) contrast indicator should not affect flow through physiologic or volume effects, (*2*) the indicator must mix with the blood uniformly, and (*3*) the indicator must remain in the intravascular space. The development of the EBCT and the introduction of nonionic contrast agents improved the ability of CT to measure regional tissue perfusion.

Ventilation Measurement Methods

Quantification of regional pulmonary ventilation has been attempted via various imaging techniques. Scintigraphic imaging (48) can measure regional ventilation as well as perfusion. Radiotracers, such as ^{133}Xe, ^{13}N, and ^{15}O, have been used tomographically for the evaluation of lung function (49). Nitrogen and oxygen have relatively short half-lives, and specialized imaging equipment is required (50). This technique yields gross estimates of ventilation within relatively large tissue volumes.

PET combined with radioactive inert gas tracer was developed to measure regional alveolar ventilation. Regional ventilation was obtained during the continuous inhalation of ^{19}Ne (51). Senda and coworkers (52) introduced a method based on the inhalation of nitrogen gas instead of ^{19}Ne. PET imaging during a constant rate intravenous infusion of nitrogen has been used to measure ventilation–perfusion ratios. Musch and coworkers (31) modified this technique to measure ventilation and perfusion separately by use of a bolus infusion of nitrogen during a short apneic period. This method has several advantages to assess both ventilation and perfusion in topological distribution: (*1*) use of a single administration of tracer, (*2*) minimal invasiveness, and (*3*) low radiation exposure to the subject. However, there are several shortcomings. First and foremost has been the fact that function is not matched with structural detail. This is being solved by the emergence of combined PET-CT scanners whereby the best of both PET and CT can be obtained if one uses state-of-the-art MDCT in conjunction with the PET side of the scanner. Often, however, the CT side is a lower level machine that is there largely to provide attenuation correction information obtained during a fairly prolonged breath hold.

Fluorescent microspheres (12) can be used to measure regional ventilation by inhaling fluorescent microsphere aerosols and measuring regional extracted dyes for each lung portion. The most significant limitation of aerosol deposition as an estimate of regional ventilation is related to the scale of measurement (53, 54). When a 1.9-cm^3 volume per piece is used, ventilation relies primarily on convective gas movement, whereas the deposition of 1.0-μm aerosol depends on gravitational settling and inertial impaction, neither of which is related to alveolar ventilation.

MRI of regional lung ventilation has been developed. T1- or T2-weighted proton MRI is significantly hampered by the low concentration of spin within the lung, susceptible artifact, and cardiac–respiratory motion (55). New methods have been introduced to increase the signal-to-noise ratio, using new contrast mechanism. The use of hyperpolarized noble gas, such as xenon-129 (56–58) or helium-3 (59–61), has been demonstrated. After the noble gas (xenon or helium) is inhaled, the airway and alveolar air space can be visualized with strong signal intensity, again demonstrated in both animals and humans.

As discussed above, one of the early limitations of clinical CT scanners was their ability to image only structure and not function, but with the increase in speed and improved spatial resolution along with the use of intravenous or intrabronchial contrast enhancement, physiologic information can be derived. Serial CT combined with nonradioactive xenon gas (atomic number, 54; K edge, 34.6 keV) has been used to measure cerebral blood flow by applying the theory proposed by Kety and Schmidt (62). Gur and coworkers (50, 63, 64) used CT with nonradioactive, radiodense xenon gas (Xe-CT) to measure regional pulmonary ventilation, taking advantage of the better spatial and temporal resolution of CT, compared with xenon scintigraphy. However, little attention was paid to careful lung volume control and the images suffered from significant misregistration problems when scans performed before and after xenon inhalation scans were subtracted from one another to visualize ventilation. Although powerful, Xe-CT techniques continue to face two primary shortcomings: (*1*) radiation dose is of growing public concern and there remains a need for methods that lower dose levels and (*2*) the need to track wash-in and/or wash-out of the gas at a fixed level of the thorax limits the current ability to image ventilation throughout the whole lung. The z-axis coverage for current MDCT scanners is at most 4 cm.

Two Xe-CT techniques for the measurement of regional pulmonary ventilation have been developed: single-breath and multibreath technique. Ball and coworkers (65) tried to measure regional ventilation by xenon scintigraphy by relating the count rate over the lung after a single breath to that after equilibration of the isotope throughout the lung. Tajik and coworkers (20) showed the potential of the single-breath method using Xe-CT, which was performed by having the subject take a single deep breath of a high nonradioactive xenon gas concentration mixture (80% xenon, 20% oxygen). Subtraction of identically gathered xenon-enhanced and unenhanced images can yield information regarding the relative distribution of local pulmonary ventilation. The enhancement due to xenon yields direct assessments of well-ventilated versus poorly ventilated lung regions. The single-breath technique has several advantages: it minimizes radiation dose and it allows for volumetric, spiral scanning. A limitation of the single-breath method lies in the fact that one must take a large breath of a high concentration of xenon. In some individuals this can cause the unwanted effect of temporarily eliminating the drive to breathe. Multibreath wash-in and/or wash-out methods offer information related to regional ventilation under dynamic conditions.

Xenon Wash-in and Wash-out Studies

X-ray CT assessments of local pulmonary ventilation have assumed monoexponential kinetics for xenon tracer gas filling or clearing the alveoli, and the model has been described by Kety (66).

Since xenon (Xe) gas was first introduced by Knipping and coworkers (67) as a contrast material to examine pulmonary function, it has been used extensively in scintigraphy (65, 68, 69), MRI (57), single-photon emission computed tomography (70), and X-ray analysis (57, 63, 65, 68–71). Stable (nonradioactive) xenon gas has a K edge similar to that of iodine and should, therefore, be a potent X-ray attenuator and provide good contrast enhancement when used in conjunction with CT scanning (72). When imaged in a conventional CT scanner, lung attenuation varies linearly with the xenon concentration in the inhaled gas (73). As discussed by Tajik and coworkers (20), the slope of the relationship between attenuation and xenon concentration was 1.55 Hounsfield units (HU) per percentage increase in xenon concentration for the electron-beam CT scanner and 2.24 HU per percentage increase in xenon concentration for the spiral/axial CT scanner. Also, attenuation is dependent on the kilovolt setting, with lower kilovolt settings giving greater attenuation because of the physical properties of xenon gas (74). Xenon is moderately soluble in blood and tissue. The Oswald solubility coefficient is 0.14 at 37°C for blood and 0.13 for fat tissue (75). The solubility of xenon gas has been considered one source of errors in the application of multibreath wash-in and/or wash-out protocols.

Errors caused by xenon solubility in blood. A number of investigators have used the Kety model in xenon scintigraphy (76, 77) and Xe-CT techniques (78), assuming xenon gas as the special case of gas with low solubility in blood. Previous studies using xenon scintigraphy reported that because of the solubility of xenon gas in blood and tissue, xenon is absorbed by the blood stream and distributed to the body parts during the wash-in phase.

Xenon wash-in and/or wash-out protocols. In the application of Xe-CT, xenon wash-in, xenon wash-out, and combined xenon wash-in/wash-out have all been used to measure cerebral blood flow in both research and clinical studies. Polacin and coworkers (79) suggested a 3-min wash-in/5-min wash-out protocol by comparing it with an 8-min wash-in protocol and evaluating precision and accuracy of the cerebral blood flow estimates. For the measurement of regional pulmonary ventilation, three protocols (20, 71, 74) have been applied in both animal and human studies, based on the Kety model, which assumes that xenon is insoluble in blood and tissue and that the xenon wash-in rate is equal to the xenon wash-out rate. Simon and coworkers (80) used a Monte Carlo simulation technique to compare the estimates of confidence interval limit in three different protocols using the Xe-CT technique. The result from Monte Carlo simulation showed that the combined wash-in/wash-out protocol gives a narrower confidence interval for the time constant with the same nominal parameters and noise level than does either wash-in or wash-out alone. Tajik and coworkers (20) showed the repeatability of the regional tracer wash-out and wash-in measurement in terms of calculated time constants. Twenty regions of interest were randomly chosen on lung base. While repeatability of wash-out measurement was performed on the basis of data obtained with the EBCT scanner, wash-in measurement repeatability was performed with the spiral/axial CT scanner. Repeatability was compared with data obtained from only one animal in the supine position. The slope was 1.01 (R^2 = 1.0) for EBCT and 1.00 (R^2 = 0.96) for spiral/axial CT.

The use of wash-in and wash-out curves to derive a single estimate of regional ventilation has been brought into question. Chon and coworkers (81) have demonstrated that the two curves do not mirror each other. These investigators have hypothesized that, because of the density of xenon gas, as the gas enters the lung and meets the lighter resident gas, Rayleigh-Taylor instabilities cause churning effects that in turn cause nonequal distribution of the inhaled gas down bifurcating paths. This observation has raised questions concerning whether inhaled xenon gas will provide the same information as inhaled helium gas. Because xenon and helium are used increasingly to study regional ventilation via polarized gas methods associated with MRI (55, 82, 83) and xenon is of increasing interest as a marker of regional ventilation assessed via CT, it is important to understand the effect of gas density and viscosity on regional ventilation. Lin and Hoffman (84) have begun to use computational fluid dynamic modeling in conjunction with airway geometry assessed via CT imaging to gain insights into these newly emerging questions.

The density and viscosity of xenon gas are 5.44 g/L and 2.25×10^{-5} Pa/s at ambient temperature, respectively (85). These values are substantially higher than those of the other gases, which may impair respiratory function when used as an inhaled anesthetic. Previous studies showed the effect of physical gas properties on pulmonary mechanics and gas exchanges, revealing that respiratory mechanics are affected by the density and viscosity of a specific gas mixture. Zhang and coworkers (86) found an increase in airway resistance related to the inspiratory xenon concentration. Because of the particularly high density and viscosity of xenon gas, the effects of a xenon–oxygen mixture on respiratory resistance are markedly sensitive to changes in the inspired xenon concentration. Rueckoldt and coworkers (87) reported a marked increase in peak air pressure and a 2.04-fold Reynolds number increase during inhalation of a 33% Xe–67% O_2 mixture, causing the zone of transition from turbulent to laminar gas flow to locate more peripherally with a consecutive increase in airway resistance.

We provide an example of the mapping of regional ventilation via Xe-CT in a prone sheep (Figure 3, *left* [p. 506]) along with a map of perfusion (Figure 3, *middle*) and $\dot{V}/\dot{Q}$ (Figure 3, *right*) in the same sheep. Specific ventilation (per minute) is color coded. Chon and coworkers (81) have interrelated wash-in and wash-out time constants to gas density and lung structure, and Marcucci and coworkers (74) have demonstrated significant differences in ventilation patterns in the prone versus supine body posture.

Ventilation–Perfusion

Much of what has been known regarding the physiology of ventilation and perfusion matching has come from early scintigraphic imaging of radioactive xenon gas (11, 88, 89). A less direct method using a multiple inert gas elimination technique was introduced by Wagner and coworkers (14). With the introduction of Xe-CT to assess regional ventilation and CT methods for assessing regional perfusion, if one carefully images an individual at the same lung volume and body posture and adjusts small mismatches in anatomy occurring between the two scanning protocols via image-warping methods (90) it becomes possible to image regional ventilation and perfusion and to map voxel-based histograms of $\dot{V}/\dot{Q}$ heterogeneity as discussed by Hoffman and coworkers (91). Kreck and coworkers (92) proposed a method for extracting regional $\dot{V}/\dot{Q}$ from a single xenon wash-in study. This model takes into account the solubility of xenon gas in blood and tissue, leading to separate measurement of ventilation, perfusion, and a ventilation–perfusion ratio. If the Hounsfield unit (X-ray attenuation coefficient) change for a given percentage of xenon gas is known, and the original regional xenon gas volume into which the inhaled xenon gas is being equilibrated, it is possible to estimate the regional density plateau that should be achieved during a wash-in maneuver. To the extent that the predicted regional density enhancement is not achieved, one can estimate regional perfusion with the assumption that the failure to achieve the predicted regional density enhancement is due to the gas being carried away by the blood. The limitation of this model is the assumption of a fixed "personal" (regional) dead space, the need for relatively high xenon radiodensity signal, and the low signal-to-noise characteristics of the perfusion signal (predicted minus actual plateau).

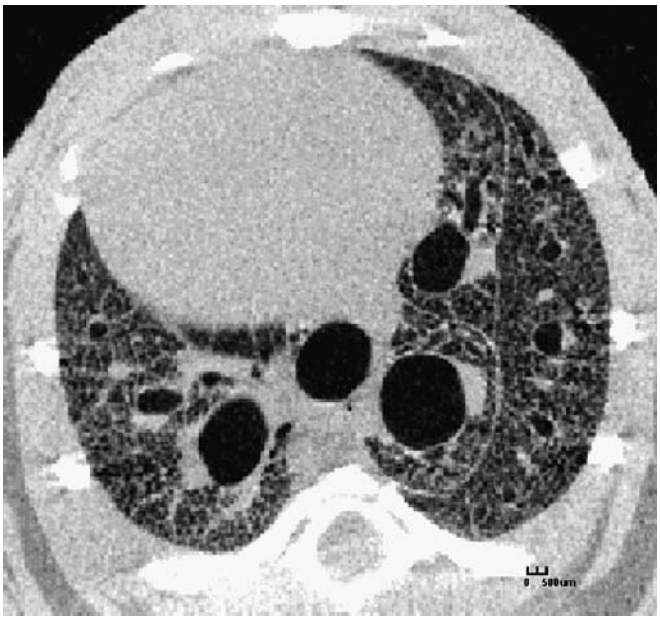

Figure 4. Cross-sectional image of a mouse lung. The mouse was imaged alive and anesthetized. With careful synchronization of respiratory events and scanner events, it is possible to image detail out to the very periphery of the lung. With careful calibration of density it becomes possible to assess regional lung air content and by imaging the lung at multiple lung volumes (airway pressures) it becomes possible to image regional "ventilation." The *inserted marker* shows a length of 500 μm.

CONCLUSIONS

MDCT in conjunction with careful gating of scanning to either respiratory or cardiac signals is now providing the ability to link structure with function in unprecedented detail. It is expected that with this new information, we will begin to gain new insights into the etiology of disease processes, devise improved methods for disease intervention, better evaluate the efficacy of these interventions, and establish phenotypes that can aid in the search for genotypes associated with many common lung pathologies. With the growing interest in the use of mouse models to help understand the genetic basis of lung disease, micro-CT (93, 94) is emerging as a powerful new tool for imaging the lung at resolutions on the order of 9 to 18 μm, which allows for the visualization of anatomic structure at the level of the alveoli in the intact mouse. As shown in Figure 4, with careful gating of scanning and respiration, it is possible to image the mouse lung such that details of the lung microstructure are clearly visible, and accurate density measures allow for assessment of regional lung function directly related to gas delivery to the lung periphery and the status of the parenchyma at the gas exchange interface.

Conflict of Interest Statement: E.A.H. is a co-owner of VIDA Diagnostics, which has marketing rights to image analysis software discussed in this article. D.C. does not have a financial relationship with a commercial entity that has an interest in the subject of this manuscript.

Acknowledgment: The authors thank all the members of the Iowa Comprehensive Lung Imaging Center (University of Iowa) who have made the work discussed here possible. The micro-CT image (Figure 4) was acquired in collaboration with Eman Namati.

References

1. Cumming G, Jones J. The construction and repeatability of lung nitrogen clearance curves. *Respir Physiol* 1966;1:238–248.
2. Secker-Walker RH, Hill RI, Markham J, Baker J, Wilhelm J, Alderson PO, Potchen EJ. The measurement of regional ventilation in man: a new method of quantitation. *J Nucl Med* 1973;14:725–732.
3. Hubmayr R, Walters B, Chevalier P, Rodarte J, Olson L. Topographical distribution of regional lung volume in anesthetized dogs. *J Appl Physiol* 1983;54:1048–1056.
4. Kallok M, Wilson T, Rodarte J, Lai-Fook S, Chevalier P, Harris L. Distribution of regional volumes and ventilation in excised canine lobes. *J Appl Physiol* 1979;47:182–191.
5. Rodarte J. Stress–strain analysis and the lung. *Fed Proc* 1982;41:130–135.
6. Chevalier P, Rodarte J, Harris L. Regional lung expansion at total lung capacity in intact vs. excised canine lungs. *J Appl Physiol* 1978;45:363–369.
7. Hoffman EA. Effect of body orientation on regional lung expansion: a computed tomographic approach. *J Appl Physiol* 1985;59:468–480.
8. Hoffman EA, Ritman EL. Effect of body orientation on regional lung expansion in dog and sloth. *J Appl Physiol* 1985;59:481–491.
9. West J, Dollery C, Hugh-jones P. The use of radiocactive carbon dioxide to measure regional blood flow in the lungs of patients with pulmonary disease. *J Clin Invest* 1961;40:1–12.
10. Hugh-Jones P, West J. Detection of bronchial and arterial obstruction by continuous gas analysis from individual lobes and segments of the lung. *Thorax* 1960;15:15–64.
11. West J, Dollery C. Distribution of blood and ventilation–perfusion ratio in the lung, measured with radioactive CO_2. *J Appl Physiol* 1960;15:405–410.
12. Robertson HT, Glenney RW, Stanford D, Mcinnes LM, Luchtel DL, Covert D. Hight-resolution maps of regional ventilation utilizing inhaled flurescent microspheres. *J Appl Physiol* 1997;82:943–953.
13. Beck KC. Regional trapping of microspheres in the lung compares well with regional blood flow. *J Appl Physiol* 1987;63:883–889.
14. Wagner PD, Saltzman HA, West JB. Measurement of continuous distributions of ventilation–perfusion ratios: theory. *J Appl Physiol* 1974;36:588–599.
15. Wood EH. Noninvasive three-dimensional viewing of the motion and anatomical structure of the heart, lungs, and circulatory system by high speed computerized X-ray tomography. *CRC Crit Rev Biochem* 1979;7:161–186.

16. Ritman EL, Kinsey JH, Robb RA, Gilbert BK, Harris LD, Wood EH. Three-dimensional imaging of the heart, lungs, and circulation. *Science* 1980;210:273–280.
17. Robb RA, Hoffman EA, Sinak LJ, Harris LD, Ritman EL. High-speed three-dimensional x-ray-computed tomography: the dynamic spatial reconstructor. *Proc IEEE* 1983;71:308–319.
18. Sinak LJ, Hoffman EA, Julsrud PR, Mair DD, Steward JB, Hagler DJ, Harris LD, Robb RA, Ritman EL. The dynamic spatial reconstructor: investigating congenital heart disease in four dimensions. *Cardiovasc Intervent Radiol* 1984;7:124–137.
19. Boyd DP, Lipton MJ. Cardiac computed tomography. *Proc IEEE* 1983;71:298–307.
20. Tajik JK, Chon D, Won C, Tran BQ, Hoffman EA. Subsecond multisection CT of regional pulmonary ventilation. *Acad Radiol* 2002;9:130–146.
21. Hoffman EA, Tajik JK, Kugelmass SD. Matching pulmonary structure and perfusion via combined dynamic multislice CT and thin-slice high-resolution CT. *Comp Med Imaging Graphics* 1995;19:101–112.
22. Wong T, Wu L, Chung N, Ritman EL. Myocardial blood flow estimated by synchronous multislice, high speed tomography. *IEEE Trans Med Imaging* 1989;8:70–77.
23. Olson LE, Hoffman EA. Heart–lung interactions determined by electron beam X-ray CT in laterally recumbent rabbits. *J Appl Physiol* 1995;78:417–427.
24. Wolfkiel CJ, Ferguson JL, Chomka EV, Law WR, Labin IN, Tenzer ML, Booker M, Brundage BH. Measurement of myocardial blood flow by ultrafast computed tomography. *Circulation* 1987;76:1262–1273.
25. Wolfkiel CJ, Rich S. Analysis of regional pulmonary enhancemant in dogs by ultrafast computed tomography. *Invest Radiol* 1992;27:211–216.
26. Nyren S, Mure M, Jacobsson H, Larsson SA, Lindahl SGE. Pulmonary perfusion is more uniform in the prone than the supine position: scintigraphy in healthy humans. *J Appl Physiol* 1999;86:1135–1141.
27. Hughes JMB, Glazier JB, Maloney JE, West JB. Effect of lung volume on the distribution of pulmonary blood flow in man. *Respir Physiol* 1968;4:58–72.
28. Melson MN, Kramer-Johansen J, Flatebo T, Muller C, Nicolaysen G. Distribution of pulmonary ventilation and perfusion measured simultaneously in awake goats. *Acta Physiol Scand* 1997;159:199–208.
29. Mijailovich SM, Treppo S, Venegas JG. Effect of lung motion and tracer kinetics corrections on PET imaging of pulmonary function. *J Appl Physiol* 1997;82:1154–1162.
30. Brudin LH, Valind S, Rhodes CG. Error analysis of combined measurement of regional ventilation and $\dot{V}/\dot{Q}$ ratio using positron emission tomography. *Phys Med Biol* 1992;37:1077–1093.
31. Musch G, Layfield JDH, Harris RS, Fischman MJ, Venegas JG. Topographical distribution of pulmonary perfusion and ventilation, assessed by PET in supine and prone humans. *J Appl Physiol* 2002;93:1841–1851.
32. Galletti GG, Venegas JG. Tracer kinetic model of regional pulmonary function using positron emission tomography. *J Appl Physiol* 2002;93:1104–1111.
33. O'Neill K, Venegas JG, Richter T, Harris RS, Layfield JDH, Musch G, Winkler T, Melo MFV. Modeling kinetic of infused ^{13}NN-saline in acute lung injury. *J Appl Physiol* 2003;95:2471–2484.
34. Markham J, Schuster DP. Effects of nonideal input functions on PET measurements of pulmonary blood flow. *J Appl Physiol* 1992;72:2495–2500.
35. Tajik JK, Kugelmass SD, Hoffman EA. An automated method for relating regional pulmonary structure and function: integration of dynamic multislice CT and thin-slice high-resolution CT. *Proc SPIE* 1993;1905:339–350.
36. Won C, Chon D, Tajik JK, Tran BQ, Robinswood GB, Beck KC, Hoffman EA. CT-based assessment of regional pulmonary microvascular blood flow parameters. *J Appl Physiol* 2003;94:2483–2493.
37. Remy-Jardin M, Mastora I, Remy J. Pulmonary embolus imaging with multislice CT. *Radiol Clin North Am* 2003;41:507–519.
38. Weiss C, Fishman EK. Multidetector 3D CT of pulmonary embolism of a peripheral intravenous line. *Emerg Radiol* 2005;11:247–249.
39. Patel S, Kazerooni EA. Helical CT for the evaluation of acute pulmonary embolism. *AJR Am J Roentgenol* 2005;185:135–149.
40. Schoepf UJ. Diagnosing pulmonary embolism: time to rewrite the textbooks. *Int J Cardiovasc Imaging* 2005;21:155–163.
41. Elias A, Cazanave A, Elias M, Chabbert V, Juchet H, Paradis H, Carriere P, Nguyen F, Didier A, Galinier M, *et al*. Diagnostic management of pulmonary embolism using clinical assessment, plasma D-dimer assay, complete lower limb venous ultrasound and helical computed tomography of pulmonary arteries: a multicentre clinical outcome study. *Thromb Haemost* 2005;93:982–988.
42. Swensen SJ. Functional CT: lung nodule evaluation. *Radiographics* 2000;20:1178–1181.
43. Levin DL, Chen Q, Zhang M, Edelman RR, Hatabu H. Evaluation of regional pulmonary perfusion using ultrafast magnetic resonance imaging. *Magn Reson Med* 2001;46:166–171.
44. Murphy D, Nicewicz J, Zabbatino S, Altin R. Local pulmonary blood flow by ultrafast computed tomography: a pilot study. *Chest* 1986;89:451S.
45. Drayer BP, Wolfson SK, Dujovny M, Rosenbaum AE, Cook EE. Physiologic changes in regional cerebral blood flow defined by xenon-enhanced CT scanning. *Neuroradiology* 1978;16:220–223.
46. Tonge KA, Mathew J, Saunderes JE. Flow rate determination using computed tomography. *Br J Radiol* 1980;53:946.
47. Guthanere DF, Nassi M, Bradley B. Validation of a CT method for flow determination: work in progress. *Radiology* 1984;151:429–432.
48. Loken MK, Medina JR, Lillehei JP, L'Heureux P, Kush GS, Ebert RV. Regional pulmonary function evaluation using xenon 133, a scintillation camera, and computer. *Radiology* 1969;93:1261–1266.
49. Ronchetti R, Ewan PW, Hughes JMP. Use of ^{13}N for regional clearance curves compared with ^{133}Xe. *Bull Physiopathol Respir (Nancy)* 1975;11:124P–125P.
50. Gur D, Shabason L, Borovetz HS, Herbert DL, Reece GJ, Kennedy WH, Serago C. Regional pulmonary ventilation measurements by xenon enhanced computed tomography: an update. *J Comput Assist Tomogr* 1981;5:678–683.
51. Valind SO, Rhodes CG, Jonson B. Quantification of reginal ventilation in man using a short-lived radiotracer: theoretical evaluation of the steady-state model. *J Nucl Med* 1987;28:1144–1154.
52. Senda M, Murata K, Itoh H, Yonekura Y, Torizuka K. Quantitative evaluation of regional pulmonary ventilation using PET and nitrogen-13 gas. *J Nucl Med* 1986;27:268–273.
53. Darquenne C, Paiva M. One dimensional simulational simulation of aerosol transport and deposition in the human lung. *J Appl Physiol* 1994;77:2889–2898.
54. Tsuda A, Butler JP, Fredberg JJ. Effects of alveolated duct structure on aerosol kinetics. *J Appl Physiol* 1994;76:2510–2516.
55. Kauczor H, Hanke A, Beek EV. Assessment of lung ventilation by MR imaging: current status and future perspectives. *Eur Radiol* 2002;12:1962–1970.
56. Albert MS, Cates GD, Driehuys B, Happer W, Saam B, Springer CJ, Wishnia A. Biological magnetic resonance imaging using laser-polarized ^{129}Xe. *Nature* 1994;370:199–201.
57. Swanson SD, Rosen MS, Coulter KP, Welsh RC, Chupp TE. Distribution and dynamics of laser-polarized ^{129}Xe magnetization *in vivo*. *Magn Reson Med* 1999;42:1137–1145.
58. Mugler JP, Driehyus B, Brookeman JR, Cates GD. MR imaging and spectroscopy using hyperpolarized ^{129}Xe gas: preliminary human results. *Magn Reson Med* 1997;37:809–815.
59. Eberle B, Weiler N, Markstaller K, Kauczor HU, Deninger A. Analysis of intrapulmonary O_2 concentration by MR imaging of inhaled hyperpolarized helium-3. *J Appl Physiol* 1999;87:2043–2052.
60. Saam BT, Yablonskiy DA, Kodibagkar VD, Leawoods JC, Gierada DS, Cooper JD, Lefrak SS, Conradi MS. MR imaging of diffusion of ^{3}He gas in healthy and diseased lungs. *Magn Reson Med* 2000;44:174–179.
61. Gierada DS, Saam B, Yablonskiy D, Cooper JD, Lefrak SS, Conradi MS. Dynamic echo planar MR imaging of lung ventilation with hyperpolarized ^{3}He in normal subjects and patients with severe emphysema. *NMR Biomed* 2000;13:176–181.
62. Kety SS, Schmidt CF. The nitrous oxide method for the quantitative determination of cerebral blood flow in man: theory, procedure, and normal value. *J Clin Invest* 1948;27:476–483.
63. Gur D, Drayer BP, Borovetz HS, Griffith BP, Hardesty RL, Wolfson SK. Dynamic computed tomography of the lung: regional ventilation measurements. *J Comput Assist Tomogr* 1979;3:749–753.
64. Gur D, Yonas H, Good WF. Local cerebral blood flow by xenon-enhanced CT: current status, potential improvements, and future directions. *Cerebrovasc Brain Metab Rev* 1989;1:68–86.
65. Ball WC Jr, Stewart PB, Newsham LG, Bates DV. Regional pulmonary function studied with xenon 133. *J Clin Invest* 1962;41:519–531.
66. Kety SS. The theory and applications of the exchange of inert gas at the lungs and tissues. *Pharmacol Rev* 1955;3:1–42.
67. Knipping HW, Bolt W, Venrath H, Valentin H, Ludes H, Endler P. A new method of heart and lung function testing, the regional functional analysis in the lung and heart clinic by the radioactive noble gas xenon 133 (isotope thoracography) [in German]. *Dtsch Med Wochenschr* 1955;80:1146–1147.

68. Bunow B, Line BR, Horton MR, Weiss GH. Regional ventilatory clearance by xenon scintigraphy: a critical evaluation of two estimation procedures. *J Nucl Med* 1979;20:703–710.
69. Mishkin FS, Brashear RE, Reese IC. Evaluation of regional perfusion and ventilation using xenon 133 and the scintillation camera. *Am J Roentgenol Radium Ther Nucl Med* 1970;108:60–70.
70. Almquist H, Jonson B, Palmer J, Valind S, Wollmer P. Regional $\dot{V}_A/\dot{Q}$ ratios in man using ^{133}Xe and single photon emission computed tomography (SPECT) corrected for attenuation. *Clin Physiol* 1999;19: 475–481.
71. Murphy DM, Nicewicz JT, Zabbatino SM, Moore RA. Local pulmonary ventilation using nonradioactive xenon-enhanced ultrafast computed tomography. *Chest* 1989;96:799–804.
72. Winkler SS, Holden JE, Sackett JF, Flemming DC, Alexander SC. Xenon and krypton as radiographic inhalation contrast media with computerized tomography: preliminary note. *Invest Radiol* 1977;12:19–20.
73. Foley WD, Haughton VM, Schmidt J, Wilson CR. Xenon contrast enhancement in computed body tomography. *Radiology* 1978;129:219–220.
74. Marcucci C, Nyhan D, Simon BA. Distribution of pulmonary ventilation using Xe-enhanced computed tomography in prone and supine dogs. *J Appl Physiol* 2001;90:421–430.
75. Isbister WH, Schofield PF, Torrance HB. Measurement of the solubility of xenon-133 in blood and human brain. *Phys Med Biol* 1965;10:243–250.
76. Susskind H, Atkins HL, Cohn SH, Ellis KJ, Richards P. Whole-body retention of radioxenon. *J Nucl Med* 1977;18:462–471.
77. Matthews CM, Dollery CT. Interpretation of ^{133}Xe lung wash-in and washout curves using and analogue computer. *Clin Sci* 1965;28:573–590.
78. Haughton VM, Donegan JH, Walsh PR, Syvertsen A, Williams AL. A clinical evaluation of xenon enhancement for computed tomography. *Invest Radiol* 1980;15:S160–S163.
79. Polacin A, Kalender WA, Eidloth H. Simulation study of cerebral blood flow measurement in xenon-CT: evaluation of washin/washout procedures. *Med Phys* 1991;18:1025–1030.
80. Simon BA, Marcucci C, Fung M, Lele SR. Parameter estimation and confidence intervals for Xe-CT ventilation studies: a Monte Carlo approach. *J Appl Physiol* 1998;84:709–716.
81. Chon D, Simon BA, Beck KC, Shikata H, Saba OI, Won C, Hoffman EA. Differences in regional wash-in and wash-out time constants for xenon-CT ventilation studies. *Respir Physiol Neurobiol* 2005;148: 65–83.
82. Beek EV, Wild J, Kauczor H, Schreiber W, Mugler JR, Lange ED. Functional MRI of the lung using hyperpolarized 3-helium gas. *J Magn Reson Imaging* 2004;20:540–554.
83. Altes TA, Rehm PK, Harrell F, Salerno M, Daniel TM, Lange ED. Ventilation imaging of the lung: comparison of hyperpolarized helium-3 MR imaging with Xe-133 scintigraphy. *Acad Radiol* 2004;11: 729–734.
84. Lin CL, Hoffman EA. A numerical study of gas transport in human lung models. *Proc SPIE* 2005;5746:92–100.
85. Viscous gases. In: Handbook of chemistry and physics, 68th ed. Cleveland, OH: CRC Press; 1987. pp. F42–F44.
86. Zhang P, Ohara A, Mashimo T, Imanaka H, Uchiyama A, Yoshiya I. Pulmonary resistance in dogs: a comparison of xenon with nitrous oxide. *Can J Anaesth* 1995;42:547–553.
87. Rueckoldt H, Vangerow B, Marx G, Haubitz B, Meyer MC, Piepenbrock S, Leuwer M. Xenon inhalation increases airway pressure in ventilated patients. *Acta Anaesthesiol Scand* 1999;43:1060–1064.
88. Milic-Emili J, Henderson J, Dolovich JAM, Trop MB, Kaneko D. Regional distribution of inspired gas in the lung. *J Appl Physiol* 1966;21: 749–759.
89. Anthonisen NR, Milic-Emili J. Distribution of pulmonary perfusion in erect man. *J Appl Physiol* 1966;21:760–766.
90. Li B, Christensen GE, McLennan G, Hoffman EA, Reinhardt JM. Establishing a normative atlas of the human lung: inter-subject warping and registration of volumetric CT. *Acad Radiol* 2003;10:255–265.
91. Hoffman EA, Reinhardt JM, Sonka M, Simon BA, Guo J, Saba O, Chon D, Samrah S, Shikata H, Tschirren J, *et al*. Characterization of the interstitial lung disease via density-based and texture-based analysis of comuputed tomography images of lung structure and function. *Acad Radiol* 2003;10:1104–1118.
92. Kreck TC, Krueger MA, Altemeier WA, Sinclair SE, Robertson HT, Shade ED, Hildebrandt J, Lamm WJ, Frazer DA, Polissar NL, *et al*. Determination of regional ventilation and perfusion in the lung using xenon and computed tomography. *J Appl Physiol* 2001;91:1741–1749.
93. Recheis W, Clough AV, Haworth ST, McLennan G, Ross AF, Hoffman EA. Imaging the mouse lung with micro-CT. In: Schuster DP, Blackwell TS, editors. Lung biology in health and disease. Vol. 203: Molecular imaging of the lungs. New York: Marcel Dekker; 2005. pp. 135–169
94. Watz H, Breithecker A, Rau WS, Kriete A. Micro-CT of the human lung: imaging of alveoli and virtual endoscopy of an alveolar duct in a normal lung and in a lung with centrilobular emphysema—initial observations. *Radiology* 2005;236:1053–1058.